Study on the influence of topography on wind shear-numerical simulation based on WRF-CALMET

Xingyu Wang[1], Yuhong Lei[1], Baolong Shi[1], Zhiyi Wang[1], Xu Li[1], Jinyan Wang[1]

[1]Key Laboratory of Climate Resource Development and Disaster Prevention in Gansu Province, College of Atmospheric Sciences, Lanzhou University, Lanzhou 730000, China

Correspondence: Jinyan Wang （wangjny@lzu.edu.cn）

Abstract

This study focuses on the critical issue of low-altitude wind shear, vital for aircraft safety during takeoff and landing. Using the WRF-CALMET model, we assess the impact of topography on low-level wind shear at Zhongchuan Airport. CALMET outperforms WRF, showing improved simulation accuracy.CALMET's simulation highlights diurnal variations in vertical wind shear, especially pronounced from 13:00 to 24:00. Notably, CALMET indicates 1-2 hazard levels higher wind shear for aircraft operations compared to WRF in a significant area.Terrain sensitivity experiments reveal CALMET's responsiveness to terrain changes during high wind shear periods, with reduced impact at higher altitudes. CALMET's incorporation of kinematic terrain influences, blocking effects, slope flow, and strengthened diversion of near-surface airflow on complex terrain contribute to these findings.This study confirms the efficacy of CALMET in simulating low-altitude wind shear, emphasizing its superiority in capturing terrain influences and reducing the aviation safety threat posed by low-altitude wind shear.

Keywords — wind shear; wind field-numerical simulation; airport; CALMET; aeronautical meteorology; topographic effect

1. Introduction

According to the definition of the International Civil Aviation Organization (ICAO), low-level windshear refers to the sharp change of spatial wind speed or direction within a 600-meter altitude range. Wind shear includes both vertical and horizontal components and typically occurs near fronts, coastlines and the surface. In the process of taking off and landing, low-level wind shear will affect the airspeed of the aircraft, causing great risks and even terrible accidents in serious cases (Evans and Turnbull, 1989). In June 1975, a Boeing 727 aircraft crashed during its landing at Kennedy Airport due to encountering low-level wind shear, resulting in 113 fatalities and 11 injuries (Fujita and Caracena, 1997); In June 2000, a Wuhan Airlines aircraft crashed during landing, also due to encountering low-level wind shear. In 2017, a

36 New Zealand Airlines A320-200 aircraft experienced low-level wind shear during
37 landing, resulting in severe damage to the aircraft and significant economic losses.
38 Therefore, accurate simulation and prediction of low-level wind shear, especially on
39 complex terrain, is of great significance for ensuring the safety of aircraft takeoffs and
40 landings at airports.

41   However, achieving accurate predictions remains a primary challenge faced by
42 numerical weather forecasting models (Colman et al., 2012). Low-level wind shear is
43 influenced by multiscale weather systems and characterized by small temporal and
44 spatial scales, high intensity, and sudden occurrences, thus making it difficult to
45 detect, study and predict. In simulating actual wind fields, simple characteristics are
46 insufficient; the wind field structure around the airport must be included. There are
47 three main methods for calculating wind shear in model wind fields (Zhang and Jia,
48 2022):1.Using meteorological radar networks and various monitoring networks
49 around airports, differential methods are employed to collect measured data,
50 recording wind speed, and wind direction in a grid format. However, these
51 measurements are scattered and small, insufficient to capture the essential
52 characteristics and dynamic development of low-level wind shear, and do not vary
53 with meteorological conditions.2.The second type of wind shear model is common in
54 engineering and consists of simple models. These typically comprise some physical
55 concepts, represented through simple mathematical fitting and basic fluid dynamics
56 solutions. They only reflect essential features of the shear wind field without fully
57 capturing the true wind field characteristics (Li et al., 2016).3.The third type of wind
58 shear model is based on atmospheric dynamics and physical equations, solved
59 directly by large computers. Among these methods, the third not only simulates the
60 real wind shear in the wind field but also provides other useful physical quantities
61 (e.g., temperature, water content, and radar reflectivity), revealing the formation
62 process, causes, and development of wind shear. Many studies have utilized
63 numerical models to simulate low-level wind shear.

64   Boilley used the non-hydrostatic Meso-NH model to simulate two different wind
65 shear events in the complex terrain around Nice Côte d'Azur Airport. They
66 successfully predicted vertical wind shear and local turbulence; however, due to the
67 model resolution limitation (500m), the study did not accurately predict the time and
68 location of low-level wind shear. Consequently, subsequent wind shear studies have
69 continuously improved spatial resolution. The Weather Research and Forecasting
70 (WRF) model, designed for high-resolution mesoscale weather forecasting, simulates
71 airflow under realistic atmospheric conditions. However, due to the grid resolution
72 of WRF being greater than 1 km, it struggles to simulate the small-scale airflow
73 movements in complex terrain. Hong Kong International Airport previously
74 attempted to predict wind shear using the WRF model, affirming its capability to
75 forecast wind shear induced by terrain changes several hours in advance and studied
76 the model's performance under non-temperature inversion conditions, it reproduced
77 wind shear characteristics well. However, providing precise warnings for the airport
78 proved challenging (Chan and Hon, 2016).Building on this, Hong Kong International
79 Airport conducted further research: using a 200m resolution numerical weather

80 prediction model, AVM, designed for fine short-term weather forecasting based on
81 WRF3.4.1 and during the whole research period, the results consistent with the
82 model forecast were observed on both runways (Hon, 2020). Since then, Hong Kong
83 International Airport improved the WRF-based coupled model, utilizing the WRF-LES
84 coupled model to capture many wind characteristics and micro-scale airflow within
85 the airport, accurately reproducing real wind direction changes (Chen et al., 2022).
86 These studies demonstrate the effectiveness of numerical models in simulating low-
87 level wind shear in airport regions, with higher resolution models providing better
88 simulation results. The series of studies conducted at Hong Kong International
89 Airport suggests that improving models based on the WRF model or coupling it with
90 other models is a promising approach for studying low-level wind shear. In previous
91 studies, the WRF/CALMET coupled model has never been used to study low-level
92 wind shear in airport regions. This study uses this model, significantly improving
93 simulation resolution and leveraging CALMET's advantages in wind field calculations,
94 providing a new method for numerical simulation of low-level wind shear in airport
95 areas.

96   Lanzhou Zhongchuan International Airport stands as one of the largest aviation
97 hubs in Northwest China, situated in the southeastern part of the Qinwangchuan
98 alluvial-fan basin, surrounded by mountains on all sides. The region is known for
99 frequent wind shear occurrences, a phenomenon that has become increasingly
100 common at Lanzhou Zhongchuan Airport due to the rapid growth in the number of
101 flights. Most wind shear events occur during spring and summer, particularly in May,
102 June, and July (Li et al., 2020). Statistical reports on wind shear at Lanzhou
103 Zhongchuan Airport indicate that the majority of incidents occur in the afternoon and
104 evening. This trend is attributed to the downward momentum in the afternoon,
105 enhanced convective activity from increased ground heating, and higher wind speeds.
106 Severe convective weather is more likely to occur in the late afternoon to evening,
107 contributing to a higher frequency of reported low-level wind shear events.
108 Conversely, fewer flights operate during the night, accompanied by reduced
109 convective weather, resulting in relatively fewer reports of aircraft encountering low-
110 level wind shear (Dang et al., 2013). In May 2016, Zhongchuan Airport installed
111 coherent Doppler lidar near the runway to study the characteristics of low-level wind
112 shear and provide warnings (Li et al., 2020). Numerical simulation studies on wind
113 shear at Zhongchuan Airport have been ongoing. Jiang L. et al. selected a 6 km×6 km
114 area near the runway at Zhongchuan Airport to establish a digital elevation model of
115 the terrain. They used FLUENT software for numerical simulation, solving iterative
116 calculations to obtain the distribution characteristics of wind speed and pressure in
117 the simulated area (Jiang et al., 2018). However, FLUENT, being a Computational
118 Fluid Dynamics (CFD) simulation software widely used in engineering, science, and
119 research fields, only considers the local turbulence of terrain and buildings on the
120 flow field. It does not account for factors such as gravity and heat exchange in real
121 atmospheric conditions. Therefore, relying solely on FLUENT for simulating and
122 warning wind shear at Zhongchuan Airport has its limitations. Improvements in
123 simulating low-level wind shear still require enhancements built upon numerical
124 weather forecasting models.

3

125   In both domestic and international research, the CALMET model is frequently
126   employed to downscale WRF, providing a finer representation of microscale terrain
127   structures. Particularly in weak wind conditions, the CALMET downscaling coupling
128   model outperforms WRF in simulating near-surface wind directions(Zhang et al.,
129   2020). The WRF/CALMET coupled system demonstrates satisfactory performance in
130   various challenging scenarios, including the complex terrain of the Qinghai-Tibet
131   Plateau(Liao et al., 2021) and the intense weather system of Super Typhoon Meranti
132   (2016)(Tang et al., 2021). Up to now, no one has used WRF/CALMET coupling system
133   to simulate and test the occurrence of low-altitude wind shear. Therefore, this study
134   leveraged the dynamic downscaling effect of the CALMET model on local micro-
135   terrain to achieve high-resolution wind shear simulations with relatively low
136   computational requirements within a small area. Additionally, we conducted
137   controlled variable experiments by modifying the original terrain. This approach has
138   not been attempted in studies investigating terrain-induced wind shear at other
139   airports. It provides an improved method for simulating low-level wind shear within
140   the WRF model.

2.Mode, Data, Method and Experimental Setup

142   2.1 Models and Experimental Setup

143   In this study, the WRF model (version 4.2) was employed to simulate a severe
144   convective weather event occurring in the vicinity of Zhongchuan Airport over a
145   duration of 96 hours, starting from July 2, 2022, at 0000 UTC. The simulated wind
146   field results were then downscaled to 100 meters through coupling with the CALMET
147   model. The model utilized a three-layer, two-way nested domain configuration
148   (Figure 1a), with horizontal grid spacings of 9 km, 3 km, and 1 km. In the vertical
149   direction, there were 39 complete Eta layers from the surface to 0 hPa. The physical
150   schemes employed by WRF are detailed in Table 1.

151
152   (a)   (b)
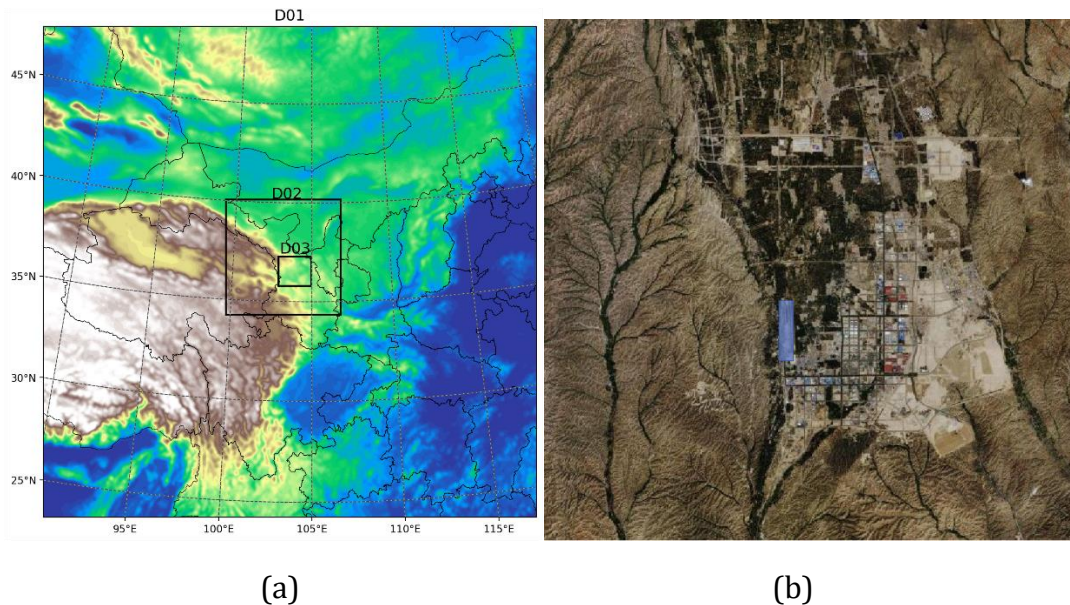
153 Figure 1. Three-layer Nested Domains of the WRF Model (a) and Simulation Area of
154 the CALMET Model © Google Maps(b), with the Zhongchuan Airport Highlighted in
155   Blue

156   Table 1. Model Configuration

Physical Scheme	WRF Option
Microphysics	Thompson graupel scheme (2-moment scheme in V3.1)
Cumulus parameterization	Tiedtke scheme
Longwave radiation	RRTMG
Shortwave radiation	RRTMG
Surface layer	Monin-Obukhov (Janjic Eta) scheme
Land surface	Noah
Boundary layer	MYJ

157   The diagnostic model utilized in this research is the CALMET model (version 6.5),
158 which constitutes the meteorological component of the California Puff Dispersion
159 Model (Scire J S.2000). In the configuration of this study, the initial guessed wind field
160 is obtained from the grid wind field generated by the innermost domain of WRF, with
161 a horizontal grid spacing of 1 km (D3 in Figure 1(a)). Since no objective analysis
162 procedure is employed, we only pay attention to the first step wind field. The
163 coverage area of the CALMET model encompasses Zhongchuan Airport and its
164 surrounding 38km×38km region (Figure 1(b)), with a horizontal resolution of 100m.
165 The vertical layers are set to 10 height levels within 600 m from the ground (the
166 height range influenced by low-level wind shear).

167   Terrain Sensitivity Experiments for Demonstrating the Impact of Terrain on
168 Wind Shear Simulation in CALMET:

169   (1) CALMET: CALMET model configured with default settings as described earlier.

170   (2) CALEMT_FLAT: Modification in the TERREL terrain processing module where
171 the elevation of all grid points is adjusted to 2000 meters. This adjustment facilitates
172 CALMET simulation on a flat underlying surface.

173   (3) CALEMT_RAISE: Modification in the TERREL terrain processing module
174 where the elevation of grid points with an altitude exceeding 2050 meters is
175 increased by 1.5 times. This modification enables CALMET to simulate wind shear
176 over a more rugged terrain.

177   These terrain sensitivity experiments are designed to showcase how variations
178 in terrain impact wind shear simulation within CALMET. The CALMET_FLAT
179 experiment simulates wind shear on a flat surface, while the CALMET_RAISE
180 experiment explores wind shear simulation over steeper terrain. The comparison of
181 results from these experiments with the default CALMET setting will provide insights
182 into the sensitivity of wind shear simulations to terrain variations.

183   2.2 data

184 The terrain data comes from the global 90 m digital elevation data set of Shuttle
185 Radar Topography (SRTM3 V4.1) of NASA, and the land use data comes from the
186 global land cover type data with 10m resolution of Pengcheng Laboratory
187 (https://data-starcloud.pcl.ac.cn/zh) of Tsinghua University in 2017.

188 The horizontal resolution of the ECMWF Reanalysis v5 (ERA5) dataset is 0.25° ×
189 0.25°, with a temporal resolution of 1 hour. This dataset is employed as both the initial
190 input and boundary fields for WRF model. Additionally, this study utilizes ERA5
191 variables, specifically geopotential height and temperature, for analyzing weather
192 systems during periods of intense convection.

193 Observational data for ground-level 10m wind speed at Lanzhou Zhongchuan
194 Airport are sourced from historical wind speed records provided by the National
195 Oceanic and Atmospheric Administration (NOAA)
196 (https://www.ncei.noaa.gov/maps/daily/) with a temporal resolution of 1 hour. The
197 ground 10m wind speed data of WRF model, CALMET model and ERA5 reanalysis
198 data are interpolated to the location of Zhongchuan Airport, and compared with the
199 observed data to verify the performance of the models.

200 2.3 method

201 To quantify the differences in 10m wind speed among the experiments, the
202 following statistical metrics are employed:

203 Index of agreement (IA):

$$204 \quad \text{IA} = 1 - \frac{\sum_{i=1}^{N} (P_i - O_i)^2}{\sum_{i=1}^{N} (|P_i - \bar{O}| + |O_i - \bar{O}|)^2} \tag{1}$$

205

206 Root-mean-squared error (RMSE):

$$207 \quad \text{RMSE} = \sqrt{\frac{1}{n} \sum_{i=1}^{n} (O_i - P_i)^2}. \tag{2}$$

208 Mean relative error (MRE):

$$209 \quad \text{MRE} = \frac{1}{n} \sum_{i=1}^{n} \frac{(P_i - O_i)}{O_i} \tag{3}$$

210 Here, $\bar{O}$ and $\bar{P}$ represent the average values of observational and simulated data,
211 respectively. Each observed value is denoted as O_i, and each simulated value is
212 denoted as P_i. Smaller values for MRE and RMSE, and an IA closer to 1.0,indicate
213 better simulation performance.

214 Wind shear can be categorized into three types: vertical shear β, meridional
215 horizontal shear α_1, and zonal horizontal shear α_2. Among these, vertical shear of
216 horizontal wind has a more significant impact on aircraft takeoff and landing

217 compared to the other types(Bretschneider et al., 2022). It results in changes in wind
218 speed and direction as an aircraft moves through different altitudes, which can lead
219 to drastic changes in airflow during ascent or descent, thereby increasing flight
220 difficulty, particularly during takeoff and landing(Keohan, 2007; Eggers et al., 2003).

3.Result

221

222   3.1 Improvement of WRF/CALMET coupling model for simulation of low-level
223 wind shear.

224   We evaluated the performance of two models in simulating near-surface wind
225 speeds, as shown in Figure 2 and Table 2. Both models showed better agreement with
226 observed data during periods of low wind speeds before convective development
227 (06:00 on July 3) and after convective cessation (02:00 on July 5). During periods of
228 intense convection, both models captured wind speed variability. Although both
229 experiments underestimated or overestimated peak wind speeds on July 3 and July 4,
230 CALMET slightly outperformed WRF in simulating high wind speeds. Furthermore,
231 Table 2 indicates that CALMET's Mean Relative Error and Root Mean Squared Error
232 were lower than those of WRF throughout the entire simulated period, with
233 improvements of 11.13% and 7.24%, respectively. CALMET's Index of Agreement
234 was also closer to 1 compared to the WRF experiment, with an improvement of
235 12.06%. These results demonstrate CALMET's superior overall simulation
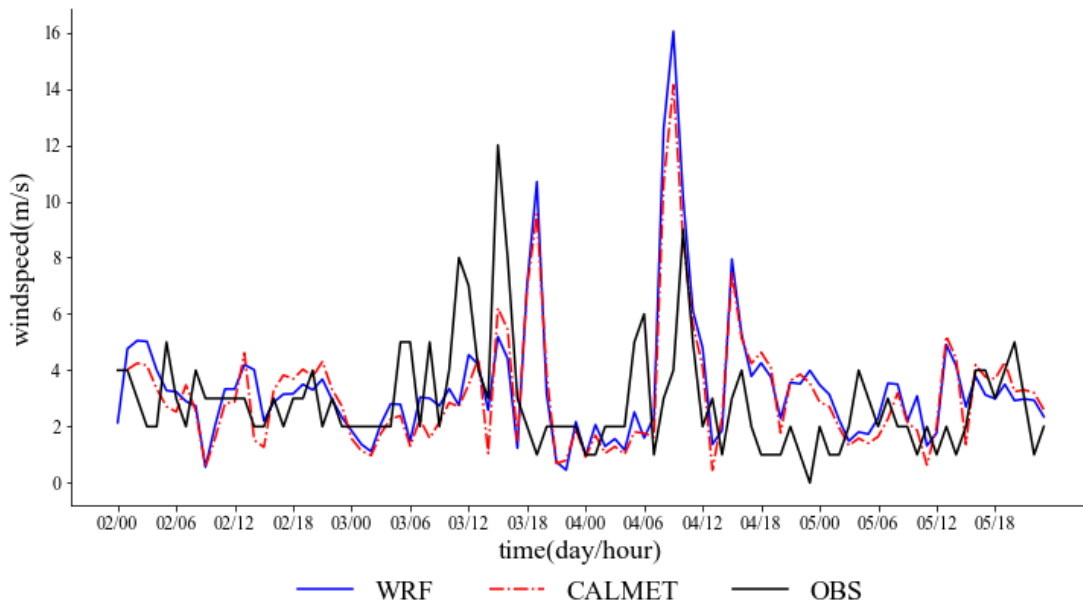236 performance compared to WRF.

237

238   Figure 2 :the time series of 10m surface wind speed for both numerical
239   simulations and observational data

240

241

242   Table 2：Statistic results of near-surface wind speed simulations in different
243   experiments averaged.

	WRF	CALMET	Improvement (%)
MRE (%)	43.255	38.425	11.13
RMSE(m /s)	2.713	2.517	7.24
IA	0.454	0.509	12.09

244   At 16:00 on July 3, significant fluctuations in surface wind speeds mark the onset
245   of convective development (Figure 2). Figure 3 illustrates the distribution of Vertical
246   Wind Shear (VWS) simulated by both models. In the layer between 10m and 30m
247   above ground level, CALMET's maximum VWS values, while consistent in location
248   with WRF's, are notably higher. Terrain analysis reveals CALMET simulates high VWS
249   values near mountain foothills and western slopes(Figure 8). WRF's high VWS values
250   primarily occur in mountainous regions. Details for the height layers of 200m-300m
251   and 500m-600m can be found in the appendix. Overall, both models exhibit
252   decreasing VWS with increasing height. From the overall distribution of VWS,
253   CALMET can simulate a wider range of third and fourth level wind shears, which are
254   associated with severe and extreme turbulence affecting aircraft takeoff and landing.
255   Furthermore, this capability provides valuable warnings for aircraft operations at
256   Nakawa Airport.

257   The atmosphere above and surrounding the mountainous terrain is
258   characterized by three distinct regions or inclined layers, comprising the thermal
259   structure undergoing diurnal variations and forming diurnal winds: slope
260   atmosphere, valley atmosphere, and mountain atmosphere (Zardi and Whiteman,
261   2013). It is challenging to observe any pure form of diurnal mountain wind system,
262   as each component interacts with the others. Well-organized thermally driven flows
263   can be identified over a broad spatial scale, ranging from the dimensions of the largest
264   mountain ranges to the smallest local topography. Therefore, concerning wind shear
265   in mountainous and foothill areas, wind shear in mountainous areas tends to be
266   smaller. When airflow passes through mountain ridges, the lower-level airflow
267   experiences significant compression. According to the conservation of flux, the
268   acceleration effect on lower-level airflow exceeds that on upper-level airflow,
269   resulting in an overall reduction in wind shear. When the acceleration effect on lower-
270   level airflow is significant while the upper-level acceleration effect is weak or absent,
271   negative wind shear occurs. Overall, the intensity of low-level wind shear may be
272   greater near mountain foothills or ridges and lesser in valleys or slopes. Hence, the
273   regions of maximum wind shear simulated by CALMET near mountain foothills or
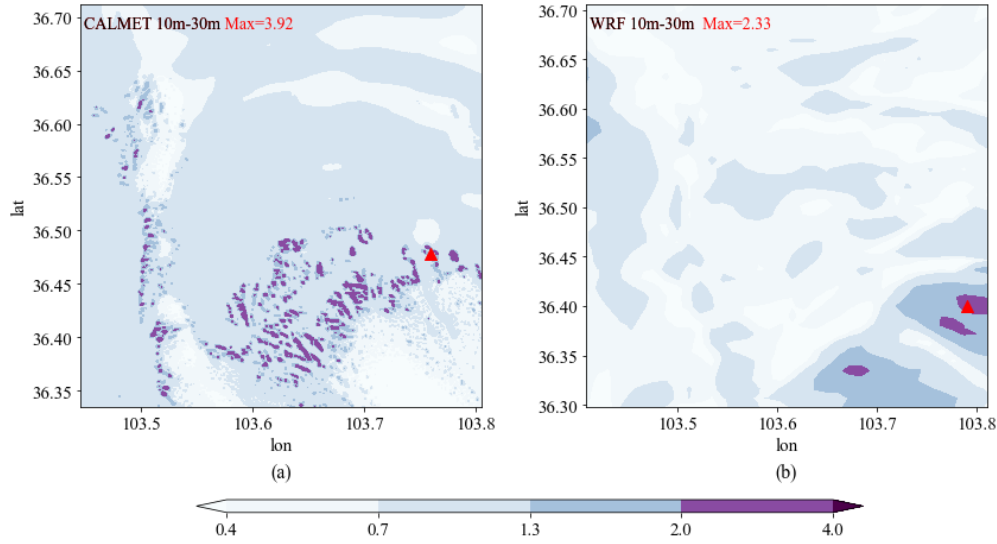274   ridges are more consistent with reality than those by WRF.

Figure 3: Vertical Wind Shear (VWS) at 16:00 on July 3, 2022, simulated by CALMET (a) and WRF (b) (Unit: m/s/10m). Triangles indicate the locations of maximum values.

Figure 4 presents the time series of maximum VWS simulated by WRF and CALMET. It can be observed that both WRF and CALMET simulations exhibit a clear diurnal pattern in maximum VWS: maximum values are relatively small around dawn and in the morning (1:00 to 12:00), with minimal fluctuations, while they increase significantly in the afternoon and evening (13:00 to 24:00), showing larger variations. However, the maximum values simulated by WRF are generally lower than those by CALMET, with this difference being more pronounced in the afternoon and evening. On July 3rd and 4th, during periods of intense convective activity, CALMET is able to simulate larger fluctuations in maximum VWS compared to normal conditions.

In summary, utilizing CALMET for downscaling WRF output of wind fields provides higher resolution and more precise surface conditions, which are advantageous for simulating mesoscale wind shear. This is primarily manifested in the following aspects: the distribution of VWS in the mid-to-low levels is more significantly influenced by terrain, and VWS decreases more rapidly with increasing altitude; the diurnal variation of maximum VWS within VWS regions follows a clear pattern and can reflect the characteristics of intense convection.

3.2 Impact of Topography on Wind Shear Simulation

Through different terrain configurations, we explored CALMET's detailed terrain impact on low-level wind shear. We found that valley winds affect VWS diurnal variation. Terrain, blocking effects, and slope flow kinematics enhance near-surface airflow diversion, deflection, and ascent over complex terrain, significantly influencing VWS, with the impact decreasing with height.

301   In the CALMET_FLAT experiment, the increase in maximum VWS during the
302   afternoon and evening is minimal (Figure 4), with slight fluctuations and values
303   around 2 m/s/10m, sometimes even lower than WRF. However, good agreement is
304   observed among the three experiments during the early morning and morning
305   periods. In CALMET_RAISE, particularly on July 3rd and 4th during intense convective
306   development, fluctuations in the afternoon and evening are more pronounced
307   compared to CALMET. However, CALMET_RAISE shows stability similar to CALMET
308   just before convective development on July 2nd, except for an unusually high value at
309   09:00 on July 4th, where fluctuations are more pronounced, but numerically close to
310   CALMET.

311   In the afternoon and evening, CALMET_FLAT shows a significant decrease in
312   maximum VWS, while CALEMT_RAISE exhibits more pronounced fluctuations. For
313   example, at 19:00 on July 3rd (Figure 5(a)-(c)), in the CALMET experiment, the
314   maximum VWS (3.56 m/s/10m) occurs in the southeastern foothills and valley areas.
315   In CALMET_FLAT, except for the absence of a high-value area in the southeast, the
316   distribution is similar to CALMET, with a maximum value of 1.77 m/s/10m in the
317   central region, which is also a flat valley area in CALMET. In CALMET_RAISE, due to a
318   sudden 1.5-fold increase in terrain elevation above 2050m, the steep terrain causes
319   chaotic wind shear distribution, with scattered high values in the central region, and
320   the maximum value increases to 4.31 m/s/10m. In summary, transitioning from
321   complex to flat terrain shifts the location of maximum VWS from mountainous areas
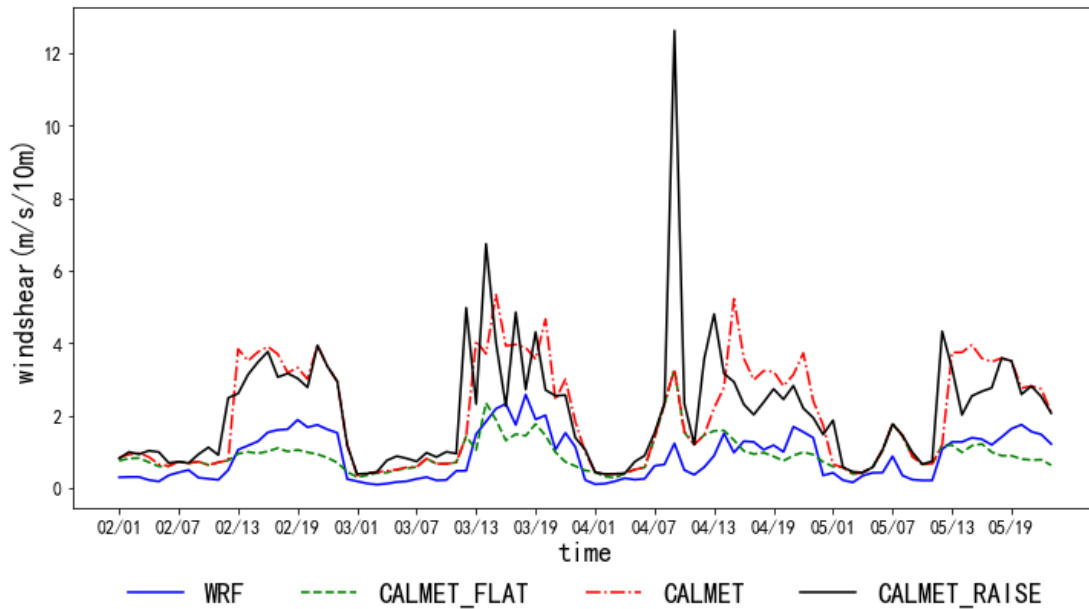322   to flat valleys.

323

324   Figure 4：Time series of 10m-30m maximum VWS values of different
325   simulation experiments in the study area

326   This phenomenon is a typical result of valley winds, driven by the interaction
327 between terrain and solar radiation. During the day, sunlight heats the surface,
328 leading to differential heating rates between slopes and valleys due to their distinct
329 topographies. Slopes, receiving direct sunlight, warm up faster than valleys. At night,
330 the surface loses heat, particularly in valleys with good heat dissipation, resulting in
331 strong nighttime cooling effects. The temperature difference between slopes and
332 valleys during the day induces upslope airflow along the slopes. As the heated air
333 ascends, airflow forms over the valleys, as depicted in Figure 5(a) where maximum
334 VWS occurs near mountainous areas. At night, cold air flows downhill along the slopes,
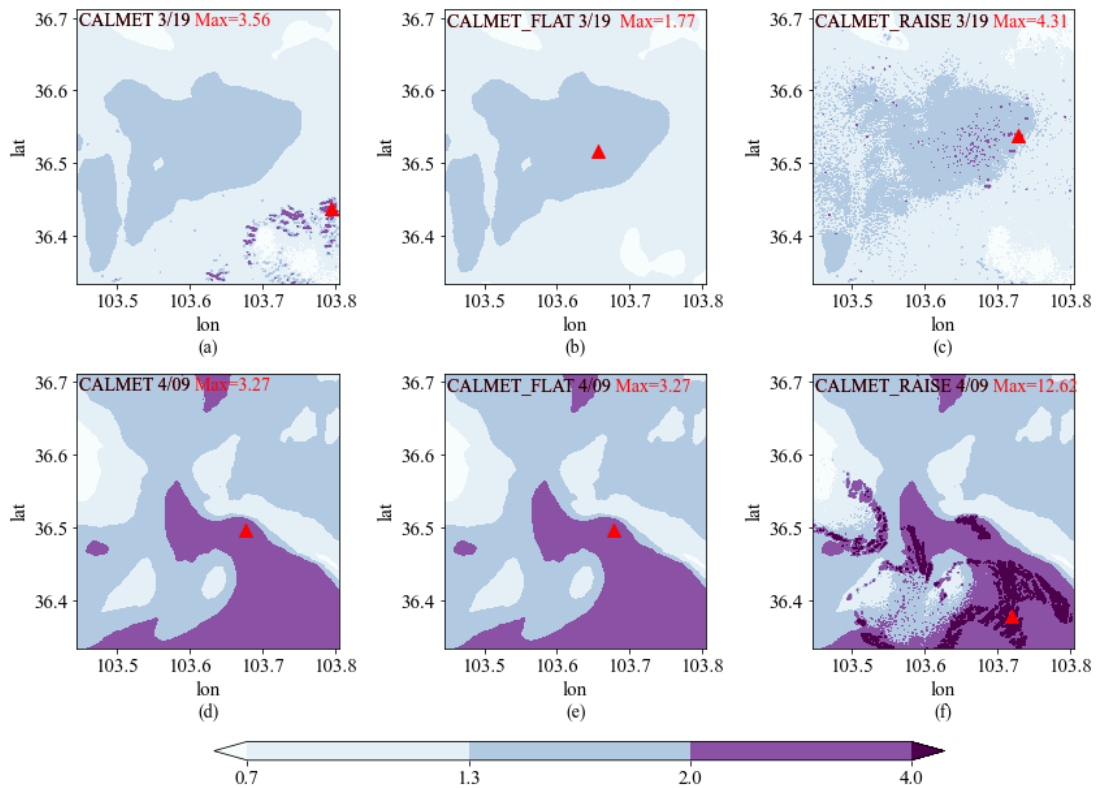335 forming downslope winds, which reverse the airflow pattern observed during the day.

336

337   Figure 5: VWS distribution of 10m-30m.(a)-(c): 19:00 on July 3, 2022; (d)-(f):
338   09:00 on 4 July 2022; (a),(d):CALMET; (b),(e):CALMET_FLAT;
339   (c),(f):CALMET_RAISE.

340   The results indicate that CALMET model simulations of VWS are highly sensitive
341 to terrain: VWS values are generally lower in flat terrain compared to complex terrain,
342 and the influence of terrain on wind shear diminishes rapidly with height. In
343 extremely steep terrain, near-surface distribution appears chaotic, but VWS values
344 notably increase above the surface compared to complex terrain. Across the three
345 experiments, the absolute differences in VWS decrease with height, suggesting a
346 diminishing impact of terrain on CALMET model simulations of VWS with increasing
347 altitude.

348   To investigate extreme high values of VWS in the CALMET_RAISE experiment at
349   09:00 on July 4th, Figures 5(d)-(f) display the VWS distribution for all experiments at
350   this time, while Figure 6 presents wind vector maps for three hours for both CALEMT
351   and CALEMT_RAISE. The VWS distribution for CALEMT and CALEMT_FLAT is similar,
352   with a peak of 3.27m/s/10m in the central region. Compared to July 3rd at 19:00,
353   both experiments show extensive high-value areas in the southeast, with
354   CALMET_RAISE reaching an exceptional maximum of 12.62m/s/10m in the
355   southeastern valley area. Additionally, CALMET_RAISE exhibits large areas of
356   exceptionally high values compared to the other experiments.

357   In Figure 6, at 08:00 and 10:00 on July 4th, the prevailing wind direction in the
358   area is northeast. Both CALMET and CALEMT_RAISE show similar wind field
359   structures, transitioning from northeast to north as terrain slopes southward. When
360   airflow passes through the southern valley, mountain ranges create denser wind
361   vectors and increased speeds. However, at 09:00, a strong northwest airflow
362   converges with the northern airflow, forming a distinct "micro-front." The terrain
363   blocking induces diversion, deflection, and upward motion of the northwesterly wind,
364   creating extensive high-value VWS areas in the southeast. Compared to CALMET,
365   CALEMT_RAISE exhibits a more chaotic wind field due to increased terrain.
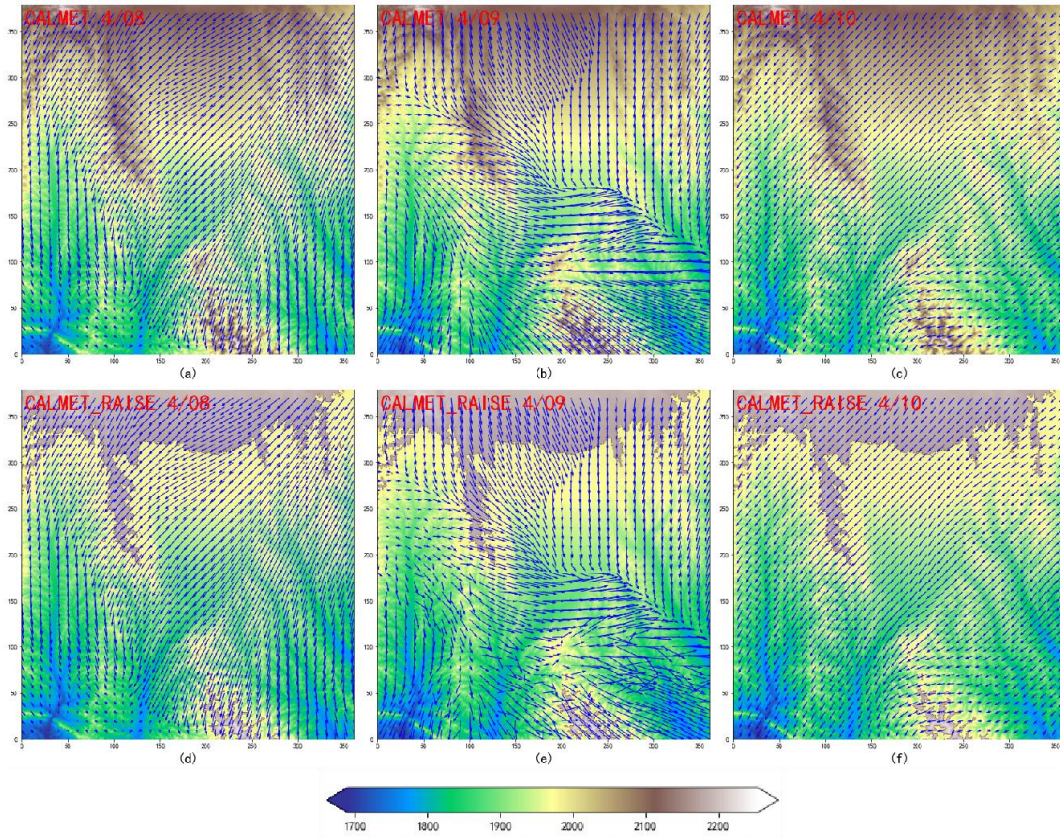

366
367   Figure 6. Topographic Elevation (unit: m) and Wind Vector Distribution. (a)-(c)
368   CALMET; (d)-(f) CALMET_RAISE; (a), (d) July 4th, 08:00; (b), (e) July 4th, 09:00; (c),
369   (f) July 4th, 10:00.

12

370   In conclusion, the widespread high-value VWS area observed at 09:00 on July 4th
371   resulted from a shift in wind direction to the northwest, encountering minimal
372   velocity reduction before reaching the tall terrain in the south, where the
373   mountainous obstruction led to diversion, deflection, and upward motion. The
374   anomalously high values in the CALEMT_RAISE experiment were attributed to the
375   elevation of the terrain, significantly intensifying the effects of diversion, deflection,
376   and upward motion. This suggests that terrain has a more pronounced impact on
377   CALMET-simulated wind shear during high wind speeds, while its influence is less
378   evident during low wind speeds. Therefore, heightened awareness of low-level wind
379   shear occurrence is warranted in complex terrain.

4 Conclusion

381   In order to investigate whether higher-resolution numerical models yield better
382   simulation results for low-level wind shear, this study focuses on a severe convective
383   weather event that occurred in the vicinity of Zhongchuan Airport on July 2, 2022.
384   The WRF/CALEMT coupled model is utilized to simulate the wind field, and the
385   influence of terrain variations on CALMET-simulated wind shear is explored. The
386   main conclusions are as follows:

387   (1) CALMET improves the simulation of near-surface winds, bringing them
388   closer to observed data than WRF, thereby facilitating more accurate modeling of
389   low-level wind shear.

390   (2) The diurnal variation of VWS shows a distinct pattern. CALMET exhibits
391   higher VWS compared to WRF, especially during the afternoon and evening. During
392   periods of intense convective activity, CALMET captures larger VWS fluctuations,
393   including higher peak values. CALMET's finer terrain features result in a VWS
394   distribution that better aligns with terrain effects, with VWS generally higher near
395   foothill areas compared to mountains, and a more pronounced decrease with altitude.

396   (3) Terrain sensitivity experiments show that during early morning and
397   morning hours, the maximum VWS of the three experiments were similar, occurring
398   in flat regions with minimal terrain influence. However, in the afternoon and evening,
399   CALMET_FLAT shows decreased maximum VWS values, while CALMET_RAISE
400   exhibits drastic fluctuations, with peak values near mountainous areas, indicating
401   significant terrain influence. Moreover, the impact of terrain on CALMET-simulated
402   VWS diminishes with altitude. These findings highlight the substantial influence of
403   terrain on CALMET, particularly during periods of high wind speeds.

404   (4) The occurrence of abnormally high VWS values in the simulations is
405   attributed to strong disturbances caused by tall terrain features: wind direction shifts
406   to northwest winds, encountering minimal reduction in wind speed before
407   encountering the tall terrain in the southern region. CALMET_RAISE elevates the
408   terrain from its original level, enhancing channeling, swirling, and updraft effects.

409   CALMET is a mature dynamic regional downscaling tool, and using other
410   numerical weather prediction models can also achieve the scale of CALMET. We chose

13

411 to use CALMET for the following reasons: from the perspective of operational
412 considerations, conducting research at the same scale requires lower computational
413 requirements and hardware needs for the CALMET model.

414   The research findings of this study are solely based on a short-term simulation
415 period of weather events in the Zhongchuan Airport area. However, this specific case
416 does not necessarily represent the overall wind shear situation at the airport, as it is
417 just one weather event with significant wind shear. And Obtaining radar wind profiler
418 data for the airport poses certain difficulties, we do not have Doppler lidar equipment
419 available. Direct observation of wind shear is challenging. We have made efforts to
420 obtain reanalysis data and site wind speed observations as much as possible. Due to
421 limited funding in the preliminary stages of our research, we could only start with
422 theoretical studies, and field experiments will be conducted once funding becomes
423 available.Our future work will expand to include longer simulation periods in more
424 airports and regions with complex terrain. This expansion aims to examine and
425 quantify the additional value provided by CALMET in simulating low-level wind shear.

426

438

References

440 Boilley A, Mahfouf J F. Wind shear over the Nice Côte d'Azur airport: case studies[J].
441 Natural Hazards and Earth System Sciences, 2013, 13(9): 2223-2238.

442 Bretschneider, L.; Hankers, R.; Schönhals, S.; Heimann, J.-M.; Lampert, A. Wind Shear
443 of Low-Level Jets and Their Influence on Manned and Unmanned Fixed-Wing Aircraft
444 during Landing Approach. *Atmosphere* **2022**, *13*, 35.
445 https://doi.org/10.3390/atmos13010035

446 Chan PW, Hon KK (2016b) Observation and numerical simulation of terrain-Induced
447 windshear at the Hong Kong International Airport in a planetary boundary layer

448 without temperature inversions. Adv Meteorol Artic ID. https:// doi.
449 org/10.1155/2016/1454513

450 Chen F, Peng H, Chan P, et al. Identification and analysis of terrain-induced low-level
451 windshear at Hong Kong International Airport based on WRF–LES combining
452 method[J]. Meteorology and Atmospheric Physics, 2022, 134(4): 60.

453 Colman B, Cook K, Snyder B J. Numerical weather prediction and weather forecasting
454 in complex terrain[M]//Mountain Weather Research and Forecasting: Recent
455 Progress and Current Challenges. Dordrecht: Springer Netherlands, 2012: 655-692.

456 Dang, B., W. Z. Sun, J. Y. Wang, et al., 2013: Analysis of low-altitude wind shear cases
457 at Lanzhou Zhongchuan Airport during 2004–2007. J. Lanzhou Univ. (Nat. Sci.), 49,
458 63–69, doi:10.3969/j.issn.0455-2059.2013.01.012. (in Chinese)

459 Eggers, A.J., Jr.; Digumarthi, R.; Chaney, K. Wind Shear and Turbulence Effects on
460 Rotor Fatigue and Load Control. *J. Sol. Energy Eng.* **2003**, *125*, 402–409.

461 Evans J, Turnbull D. Development of an automated windshear detection system using
462 Doppler weather radar[J]. Proceedings of the IEEE, 1989, 77(11): 1661-1673.

463 Fujita T T, Caracena F. An analysis of three weather-related aircraft accidents[J].
464 Bulletin of the American Meteorological Society, 1977, 58(11): 1164-1181.

465 Hon K K. Predicting low-level wind shear using 200-m-resolution NWP at the Hong
466 Kong International Airport[J]. Journal of Applied Meteorology and Climatology, 2020,
467 59(2): 193-206.

468 Jiang Lihui, Liu Xiaoyu, Li Zhen, et al. Study on the influence of terrain and buildings
469 around Lanzhou Zhongchuan Airport on wind field [J]. Computer and Digital
470 Engineering, 2018, 46(3): 561-565,626.

471 Keohan, C. Ground-based wind shear detection systems have become vital to safe
472 operations. *ICAO J.* **2007**, *62*, 16–19, 33–34.

473 Liao R, Fang X, Liu H, et al. Wind characteristic in the complex underlying terrain as
474 studied with CALMET system[C]//Journal of Physics: Conference Series. IOP
475 Publishing, 2021, 2006(1): 012053.

476 Li Hai, Zhou Meng, Guo Qinghua , Wu Renbiao , Xi Jiangtao. Compressive sensing-
477 based wind speed estimation for low-altitude wind-shear with airborne phased array
478 radar[J], Multidimensional Systems and Signal Processing,2016,7:1-14

479 Li L, Shao A, Zhang K, et al. Low-level wind shear characteristics and lidar-based
480 alerting at lanzhou zhongchuan international airport, China[J]. Journal of
481 Meteorological Research, 2020, 34(3): 633-645.

482 Roland, J. White Effect of wind shear on airspeed during airplane landing approach. *J.
483 Aircr.* **1992**, *29*, 237–242.

484   Scire J S, Robe F R, Fernau M E, et al. A user's guide for the CALMET Meteorological
485   Model[J]. Earth Tech, USA, 2000, 37.

486   Tang S, Huang S, Yu H, et al. Impact of horizontal resolution in CALMET on simulated
487   near-surface wind fields over complex terrain during Super Typhoon Meranti
488   (2016)[J]. Atmospheric Research, 2021, 247: 105223.

489   Zardi, D., Whiteman, C.D. (2013). Diurnal Mountain Wind Systems. In: Chow, F., De
490   Wekker, S., Snyder, B. (eds) Mountain Weather Research and Forecasting. Springer
491   Atmospheric Sciences. Springer, Dordrecht. https://doi.org/10.1007/978-94-007-
492   4098-3_2

493   Zhang D, Chen L, Zhang F, et al. Numerical simulation of near-surface wind during a
494   severe wind event in a complex terrain by multisource data assimilation and dynamic
495   downscaling[J]. Advances in Meteorology, 2020, 2020: 1-14.

496   Zhang Y, Jia M. Low-level wind shear of wind field modeling and simulation[J]. 2022.